Neutron-induced γ-ray production cross sections for the first excited-state transitions in ^{20}Ne and ^{22}Ne

S. MacMullin,[1,2,*] M. Boswell,[3] M. Devlin,[3] S. R. Elliott,[3] N. Fotiades,[3] V. E. Guiseppe,[4] R. Henning,[1,2] T. Kawano,[3] B. H. LaRoque,[3,†] R. O. Nelson,[3] and J. M. O'Donnell[3]

[1]*Department of Physics and Astronomy, University of North Carolina, Chapel Hill, North Carolina 27599, USA*
[2]*Triangle Universities Nuclear Laboratory, Durham, North Carolina 27708, USA*
[3]*Los Alamos National Laboratory, Los Alamos, New Mexico 87545, USA*
[4]*Department of Physics, University of South Dakota, Vermillion, South Dakota 57069, USA*

(Received 4 October 2012; published 21 December 2012)

Background: Neutron-induced reactions are a significant concern for experiments that require extremely low levels of radioactive backgrounds. Measurements of γ-ray production cross sections over a wide energy range help to predict and identify neutron backgrounds in these experiments.

Purpose: The purpose of this experiment is to determine partial γ-ray production cross sections for neutron-induced reactions in natural neon.

Methods: The broad spectrum neutron beam at the Los Alamos Neutron Science Center (LANSCE) was used for the measurement. Gamma rays from neutron-induced reactions were detected using the GErmanium Array for Neutron Induced Excitations (GEANIE).

Results: Partial γ-ray cross sections were measured for the first excited-state transitions in ^{20}Ne and ^{22}Ne. The measured cross sections were compared to the TALYS and CoH_3 nuclear reaction codes.

Conclusions: These are the first experimental data for (n, n') reactions in neon. In addition to providing data to aid in the prediction and identification of neutron backgrounds in low-background experiments, these new measurements will help refine cross-section predictions in a mass region where models are not well constrained.

DOI: 10.1103/PhysRevC.86.067601 PACS number(s): 25.40.Fq, 23.40.−s, 27.30.+t, 95.35.+d

Several current and next-generation detectors designed to search for weakly interacting massive particle (WIMP) dark matter will make use of large volumes of noble liquids (Ne, Ar, Xe) [1]. For example, the DEAP/CLEAN experimental program uses either argon or neon [2–5]. The detectors are designed to measure the scintillation light from putative WIMP-nucleus scattering. Although electrons and γ rays, which scatter from atomic electrons, are well discriminated from nuclear recoils, neutrons, which scatter from nuclei in the detector, will mimic WIMP signals [6]. These scattering neutrons contribute an irreducible background that has to be quantified using calibration data and Monte Carlo simulations. For the latter, it is crucial that neutron scattering cross sections are well known.

In nuclear reaction codes used to predict γ-ray production cross sections, the optical model determines transmission coefficients, which are used in statistical calculations to determine cross sections. The optical model is known to provide an excellent phenomenological description of nucleon-nucleus scattering for medium mass and heavy nuclei ($A > 24$) over a wide energy range ($E < 200$ MeV) [7]. Global optical models are based on a unique functional form for the energy and mass dependence of the potential depths, with physically constrained parameters that describe nuclear radii and surface diffuseness. The limited range of the global optical-model potentials is largely due to the limited experimental data in the light-to-medium-mass range [8].

We have measured the partial γ-ray production cross sections for the first excited-state transitions in ^{20}Ne and ^{22}Ne for incident neutron energies up to 16 MeV. These are the first experimental data for (n, n') reactions in neon. The inclusion of these cross sections over a wide energy range in Monte Carlo codes will help in predicting neutron backgrounds in dark matter experiments that use neon as a target. These data will also provide an additional benchmark for global optical-model parameters. This work is a continuation of previous experiments which measured $(n, xn\gamma)$ reactions in lead [9], copper [10], and argon [11].

Data were collected at the Los Alamos Neutron Science Center (LANSCE) [12]. The γ rays produced in neutron-induced reactions were measured with the the GErmanium Array for Neutron Induced Excitations (GEANIE) [13]. GEANIE is located 20.34 m from the Weapons Neutron Research facility (WNR) spallation neutron source on the 60°-right flight path. A broad-spectrum (∼0.2–800 MeV) pulsed neutron beam was produced via spallation on a ^{nat}W target by an 800-MeV proton linear accelerator beam. The proton beam structure contained 625-μs-long "macropulses" repeated at 60 Hz, or every 16.7 ms. One in three macropulses was delivered to another facility, resulting in an average rate of 40 s^{-1}. Each macropulse consisted of "micropulses" spaced every 1.8 μs, each less than 1 ns long. The pulsed beam allowed incident neutron energies to be determined using the time-of-flight technique. During the experimental runs, 1.2×10^{10} micropulses produced about 1.2×10^{12} neutrons of energies from 1 to

*spm@physics.unc.edu
†Current address: Department of Physics, University of California, Santa Barbara, CA 93106, USA.

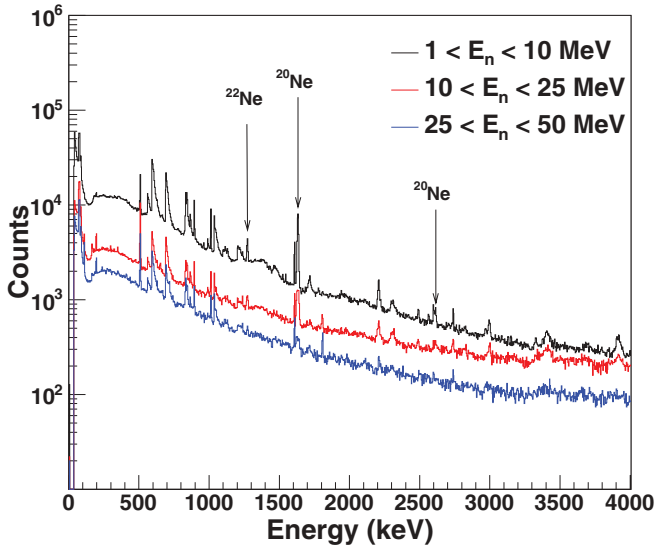

FIG. 1. (Color online) Neon-sample γ-ray spectra selected for different neutron energy windows. The spectrum shown in black (top) corresponds to $1 < E_n < 10$ MeV. The spectrum shown in red (middle) corresponds to $10 < E_n < 25$ MeV. The spectrum shown in blue (bottom) corresponds to $25 < E_n < 50$ MeV. The observed excited-state transitions in ^{20}Ne and ^{22}Ne are labeled.

100 MeV on target to be used in the cross-section analysis. The neutron flux on target was measured with an in-beam fission ionization chamber with ^{235}U and ^{238}U foils [14] located about 2 m upstream from the center of the GEANIE array.

GEANIE comprises 20 high-purity germanium detectors with bismuth germinate (BGO) escape suppression shields. Detectors have either a planar or coaxial geometry and are typically operated with maximum γ-ray energy ranges of 1 and 4 MeV, respectively. Because almost all of the excited states in neon produce γ rays with energies greater than 1 MeV, the planar detectors were removed from the data processing chain to reduce dead time. The data from five out of nine of the the coaxial detectors with good energy resolution and timing information were used for the cross-section analysis.

The neon gas target cell was a 3.81-cm-diameter and 6.35-cm long thin-walled aluminum cylinder with 0.127-mm-thick Kapton windows at either end. The gas cell was placed at the center of the GEANIE array, with the neutron beam passing through the Kapton foils. The ^{nat}Ne gas pressure was maintained at 3.96 atm with less than 1% variation over the course of the experiment.

Partial γ-ray cross sections were determined using the same method described in Ref. [11]. Neon-sample γ-ray spectra selected for specific neutron energy windows are shown in Fig. 1. All γ-ray lines present in the data have been identified. Partial γ-ray cross sections were determined for the $E_\gamma = 1633.7$-keV $2^+ \rightarrow 0$ transition in ^{20}Ne and the $E_\gamma = 1274.5$-keV $2^+ \rightarrow 0$ transition in ^{22}Ne. The $E_\gamma = 2613.8$-keV $4^+ \rightarrow 2$ transition in ^{20}Ne was visible in the data, but only over a broad energy bin. In the case of ^{20}Ne, most of the levels above the 4966.5-keV 2^- state have a large branching ratio for decay by α-particle emission. TALYS [15] calculations indicate that for an 8-MeV neutron about 35% of the total inelastic cross section will not be seen in γ rays because of competition with the α branch.

Most of the other γ-ray lines were attributed to backgrounds from the sample cell (^{27}Al) or neutron inelastic scattering in germanium or bismuth (from the BGO shields). Because the duty cycle was only about 2.5%, uncorrelated backgrounds were negligible compared to beam-induced events. Although there were some ^{214}Bi γ rays from radon decay near the observed neon lines, they were not visible in the beam-on data.

We assumed that the observed γ ray at 1633 keV was due only to the ^{20}Ne$(n, n'\gamma)^{20}$Ne reaction. Considering that neon is 90.48% ^{20}Ne, 9.25% ^{22}Ne, and 0.27% ^{21}Ne, the only other reactions that could produce ^{20}Ne are ^{21}Ne$(n, 2n\gamma)^{20}$Ne or ^{22}Ne$(n, 3n\gamma)^{20}$Ne. The low isotopic abundance of ^{21}Ne makes the ^{21}Ne$(n, 2n\gamma)^{20}$Ne reaction unlikely to be seen.

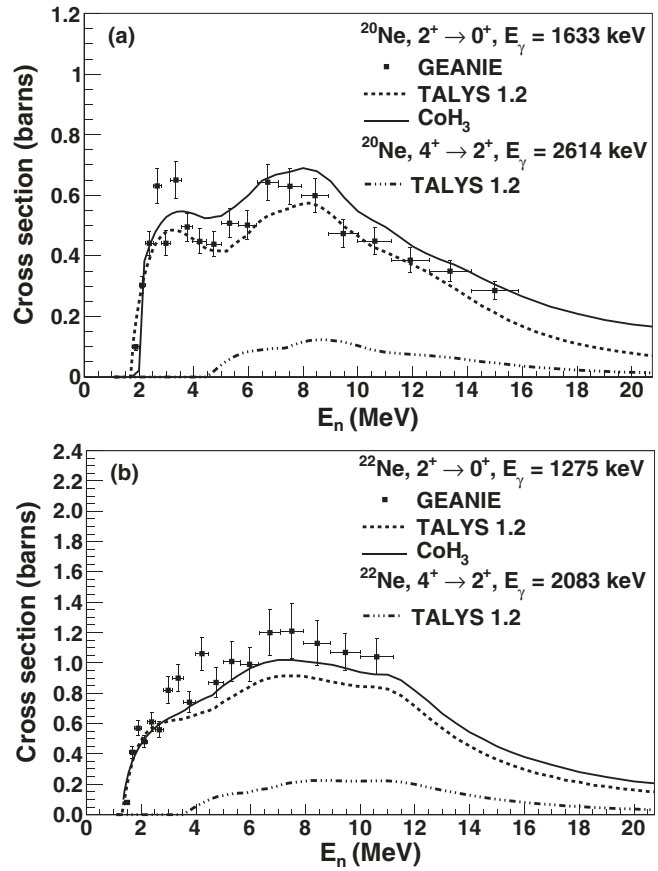

FIG. 2. (a) Partial γ-ray cross section for ^{20}Ne. Data from the $2^+ \rightarrow 0^+$ first excited-state transition are compared with the TALYS and CoH_3 calculations. A TALYS calculation for the $4^+ \rightarrow 2^+$ second excited-state transition is also shown. (b) Partial γ-ray cross section for ^{22}Ne. Data from the $2^+ \rightarrow 0^+$ first excited-state transition are compared with the TALYS and CoH_3 calculations. A TALYS calculation for the $4^+ \rightarrow 2^+$ second excited-state transition is also shown.

The ^{22}Ne$(n, 3n\gamma)^{20}$Ne does not contribute to the measured cross section because it has a threshold of more than 20 MeV. Similarly, the 1275-keV transition observed from ^{22}Ne was assumed to be from the ^{22}Ne$(n, n'\gamma)^{22}$Ne reaction. Cross sections were measured from threshold to where they fall below our detection sensitivity. The measured cross sections are shown in Fig. 2 and are listed in Tables I and II.

The TALYS [15] and CoH_3 [16,17] nuclear reaction codes were used to predict the γ-ray production cross sections for the transitions studied in the present work. The TALYS calculation used a direct reaction model using the global optical-model parametrization of Koning and Delaroche [8], a pre-equilibrium model, and a Hauser-Feshbach statistical calculation. It included discrete level information, based on the ENSDF [18] data for the first 30 levels. The CoH_3 code included discrete level information for the first 47 levels, up to the 11.32-MeV 2^+ state in ^{20}Ne. Because neon is a deformed nucleus ($\beta_2 = 0.73$ for ^{20}Ne and $\beta_2 = 0.63$ for ^{22}Ne), the CoH_3 code used a Hauser-Feshbach calculation, including transmission coefficients obtained from a coupled-channels calculation [19]. Although CoH_3 reproduced the data more accurately than TALYS, the discrepancy between the CoH_3 calculation and the data is most likely due to the use of the spherical Koning-Delaroche potential in the coupled-channels calculation. A better model calculation could be made if more experimental data for neutron scattering become available. The peaks in the ^{20}Ne cross section around 3 MeV are due to resonances. Neither the TALYS calculations nor the CoH_3 calculations reproduce the structure, but rather give the average behavior of the cross section.

The fact that only the first excited-state transitions in ^{20}Ne and ^{22}Ne were observed in the γ-ray data has potential implications for neon-based dark matter experiments. Although neutron elastic scattering can mimic a WIMP signal, experiments may be able to discriminate against inelastic scattering if one or more coincident γ rays are produced. While the cross sections for the first excited-state transitions in ^{20}Ne and ^{22}Ne are relatively large, TALYS calculations, shown in Fig. 2, indicate that the γ-ray production cross sections from second excited-state transitions in both ^{20}Ne and ^{22}Ne are at least a factor of 5 smaller for neutron energies less than about 10 MeV. In addition, because of the large α-particle decay branch, levels higher than the 4966.5-keV 2^- state in ^{20}Ne are unlikely to be seen through γ-ray emission. However, because the α particle will have a short range and produce a large amount of scintillation light in the detector, it may provide a very clean tag for these neutrons.

In addition to using γ rays or α particles from neutron inelastic scattering as an active veto, if the rate of inelastic scattering in the detector's sensitive volume can be measured, the background from neutron elastic scattering may be estimated if both the elastic and inelastic cross sections are known. In most underground experiments, the dominant source of neutrons is those produced from naturally occurring isotopes in the ^{238}U and ^{232}Th decay chains. Alpha particles produced in these decays undergo (α, n) reactions and produce neutrons in the 1 to 10 MeV range. The ratios of the elastic scattering to

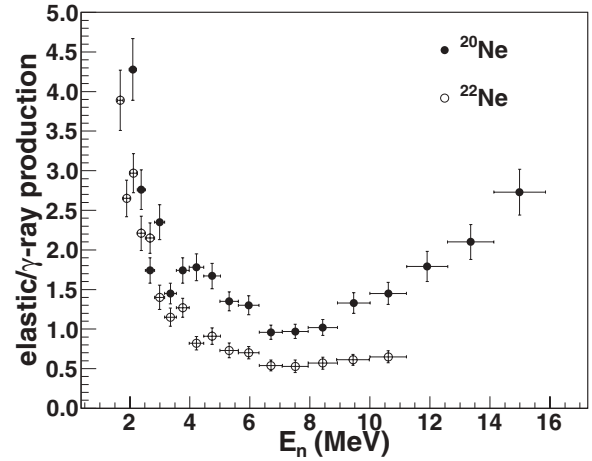

FIG. 3. The ratio of the elastic scattering cross section to the γ-ray production cross section. The solid circles correspond to ^{20}Ne and the open circles correspond to ^{22}Ne.

γ-ray production cross sections for ^{20}Ne and ^{22}Ne are shown in Fig. 3 and are listed in Table III. The elastic scattering cross section was calculated using TALYS, which used the Koning-Delaroche global optical model including a compound nucleus cross section using a Hauser-Feshbach statistical calculation with a Moldauer width fluctuation correction factor [20,21]. The γ-ray production cross section corresponds to the values measured in the current experiment. Because there are currently no experimental data for elastic scattering in neon to use for comparison, the error bars only represent the current experiment. Although the ratio of the cross sections becomes large as the neutron energy approaches threshold, only about 15% of the total neutrons produced from ^{238}U and ^{232}Th-induced (α, n) reactions have energies below 2 MeV [22].

We have measured neutron-induced γ-ray production cross sections for the first excited-state transitions in ^{20}Ne and ^{22}Ne from threshold to as high as 16 MeV, where they fall below our detection sensitivity. The measured cross sections will aid in the identification and discrimination of neutrons in underground experiments which use neon as a detector. Because these are the first experimental data for (n, n') reactions in neon, they will enrich the nuclear databases and provide a useful benchmark in a mass region where the optical model is not well constrained.

This work was supported in part by Laboratory Directed Research and Development at Los Alamos National Laboratory, National Science Foundation Grant No. 0758120, and US Department of Energy Grant No. 2013LANLE9BW. This work benefited from the use of the Los Alamos Neutron Science Center, funded by the US Department of Energy under Contract No. DE-AC52-06NA25396. R.H. and S.M. are supported by DOE ONP Grants No. DE-FG02-97ER4104 and No. DE-FG02-266 97ER41033. V.E.G. is supported by DOE ONP Grant No. DE-SCOO05054.

APPENDIX: PARTIAL γ-RAY CROSS SECTIONS

TABLE I. ^{20}Ne$(n, n'\gamma)^{20}$Ne $2^+ \rightarrow 0^+$ $E_\gamma = 1633$ keV.

E_n (MeV)	σ_{data} (barn)	σ_{TALYS} (barn)	σ_{CoH_3} (barn)
1.9 ± 0.1	0.10 ± 0.01	0.19	0.13
2.1 ± 0.1	0.30 ± 0.03	0.31	0.30
2.4 ± 0.1	0.44 ± 0.04	0.39	0.44
2.7 ± 0.2	0.63 ± 0.06	0.45	0.49
3.0 ± 0.2	0.44 ± 0.04	0.48	0.53
3.4 ± 0.2	0.65 ± 0.06	0.49	0.55
3.8 ± 0.2	0.50 ± 0.05	0.47	0.54
4.2 ± 0.2	0.45 ± 0.04	0.44	0.53
4.7 ± 0.3	0.44 ± 0.04	0.42	0.53
5.3 ± 0.3	0.51 ± 0.05	0.43	0.56
6.0 ± 0.3	0.50 ± 0.05	0.48	0.60
6.7 ± 0.4	0.64 ± 0.06	0.53	0.66
7.5 ± 0.4	0.63 ± 0.06	0.56	0.68
8.4 ± 0.5	0.60 ± 0.06	0.57	0.68
9.5 ± 0.5	0.47 ± 0.05	0.50	0.59
10.6 ± 0.6	0.45 ± 0.04	0.43	0.52
11.9 ± 0.7	0.39 ± 0.04	0.38	0.43
13.4 ± 0.7	0.35 ± 0.04	0.31	0.37
15.0 ± 0.8	0.29 ± 0.03	0.22	0.31

TABLE II. ^{22}Ne$(n, n'\gamma)^{22}$Ne $2^+ \rightarrow 0^+$ $E_\gamma = 1275$ keV.

E_n (MeV)	σ_{data} (barn)	σ_{TALYS} (barn)	σ_{CoH_3} (barn)
1.5 ± 0.1	0.08 ± 0.01	0.00	0.25
1.7 ± 0.1	0.41 ± 0.04	0.34	0.36
1.9 ± 0.1	0.57 ± 0.05	0.46	0.44
2.1 ± 0.1	0.48 ± 0.04	0.53	0.49
2.4 ± 0.1	0.61 ± 0.06	0.58	0.55
2.7 ± 0.2	0.56 ± 0.05	0.61	0.60
3.0 ± 0.2	0.82 ± 0.09	0.63	0.63
3.4 ± 0.2	0.90 ± 0.09	0.63	0.67
3.8 ± 0.2	0.74 ± 0.07	0.65	0.72
4.2 ± 0.2	1.06 ± 0.11	0.65	0.78
4.7 ± 0.3	0.87 ± 0.10	0.71	0.80
5.3 ± 0.3	1.01 ± 0.13	0.78	0.90
6.0 ± 0.3	0.99 ± 0.11	0.85	0.97
6.7 ± 0.4	1.20 ± 0.15	0.91	1.02
7.5 ± 0.4	1.21 ± 0.18	0.92	1.02
8.4 ± 0.5	1.13 ± 0.15	0.90	1.00
9.5 ± 0.5	1.07 ± 0.12	0.86	0.96
10.6 ± 0.6	1.04 ± 0.12	0.84	0.92

TABLE III. The ratio of the elastic scattering cross section to the measured γ-ray production cross section for ^{20}Ne and ^{22}Ne.

E_n (MeV)	^{20}Ne	^{22}Ne
1.5 ± 0.1		21.2 ± 2.6
1.7 ± 0.1		3.9 ± 0.4
1.9 ± 0.1	13.9 ± 1.4	2.7 ± 0.2
2.1 ± 0.1	4.3 ± 0.4	3.0 ± 0.2
2.4 ± 0.1	2.8 ± 0.3	2.2 ± 0.2
2.7 ± 0.2	1.7 ± 0.2	2.2 ± 0.2
3.0 ± 0.2	2.4 ± 0.2	1.4 ± 0.2
3.4 ± 0.2	1.5 ± 0.1	1.2 ± 0.1
3.8 ± 0.2	1.7 ± 0.2	1.3 ± 0.1
4.2 ± 0.2	1.8 ± 0.2	0.82 ± 0.08
4.7 ± 0.3	1.7 ± 0.2	0.9 ± 0.1
5.3 ± 0.3	1.4 ± 0.1	0.73 ± 0.09
6.0 ± 0.3	1.3 ± 0.1	0.70 ± 0.08
6.7 ± 0.4	0.96 ± 0.09	0.54 ± 0.07
7.5 ± 0.4	0.97 ± 0.09	0.53 ± 0.08
8.4 ± 0.5	1.0 ± 0.1	0.57 ± 0.08
9.5 ± 0.5	1.3 ± 0.1	0.61 ± 0.07
10.6 ± 0.6	1.5 ± 0.1	0.65 ± 0.07
11.9 ± 0.7	1.8 ± 0.2	
13.4 ± 0.7	2.1 ± 0.2	
15.0 ± 0.8	2.7 ± 0.3	

[1] G. Bertone, *Particle Dark Matter* (Cambridge University Press, New York, 2010).
[2] M. G. Boulay, A. Hime, and J. Lidgard, arXiv:nucl-ex/0410025.
[3] M. Boulay and B. Cai, J. Phys.: Conf. Ser. **136**, 042081 (2008).
[4] D. N. McKinsey, Nucl. Phys. B, Proc. Suppl. **173**, 152 (2007).
[5] A. Hime, in Proceedings of the DPF-2011 Conference, Providence, RI, August 8–13, 2011, arXiv:1110.1005.
[6] M. G. Boulay and A. Hime, Astropart. Phys. **25**, 179 (2006).
[7] P. E. Hodgson, *The Optical Model of Elastic Scattering* (Clarendon, Oxford, 1963).
[8] A. J. Koning and J. P. Delaroche, Nucl. Phys. A **713**, 231 (2003).
[9] V. E. Guiseppe *et al.*, Phys. Rev. C **79**, 054604 (2009).
[10] M. Boswell *et al.*, 2010 Fall Meeting of the APS Division of Nuclear Physics, Santa Fe, NM http://meetings.aps.org/link/BAPS.2010.DNP.GD.4.
[11] S. MacMullin *et al.*, Phys. Rev. C **85**, 064614 (2012).

[12] P. W. Lisowski *et al.*, Nucl. Sci. Eng. **106**, 208 (1990).
[13] N. Fotiades *et al.*, Phys. Rev. C **69**, 024601 (2004).
[14] S. A. Wender *et al.*, Nucl. Instrum. Methods Phys. Res., Sect. A **336**, 226 (1993).
[15] A. J. Koning, S. Hilaire, and M. C. Duijvestijn, *"TALYS-1.0", Proceedings of the International Conference on Nuclear Data for Science and Technology, April 22-27, 2007, Nice, France*, edited by O. Bersillon, F. Gunsing, E. Bauge, R. Jacqmin, and S. Leray (EDP Sciences, Les Ulis, France, 2008), pp. 211–214.
[16] T. Kawano, CoH: The Hauser-Feshbach-Moldauer statistical model with the coupled-channels theory, Los Alamos National Laboratory, unpublished, 2003.
[17] T. Kawano *et al.*, J. Nucl. Sci. Technol. **47**, 462 (2010).
[18] D. R. Tilley *et al.*, Nucl. Phys. A **636**, 247 (1998); R. Firestone, Nucl. Data Sheets **106**, 1 (2005). Data extracted from the ENSDF database, revision of Oct. 19, 2012, http://www.nndc.bnl.gov/ensdf/.
[19] T. Kawano, P. Talou, J. E. Lynn, M. B. Chadwick, and D. G. Madland, Phys. Rev. C **80**, 024611 (2009).
[20] P. A. Moldauer, Phys. Rev. C **14**, 764 (1976).
[21] P. A. Moldauer, Nucl. Phys. A **344**, 185 (1980).
[22] D.-M. Mei, C. Zhang, and A. Hime, Nucl. Instrum. Methods Phys. Res., Sect. A **606**, 651 (2009); neutronyield.usd.edu.